Comparing Images of ICRF Sources at X-, K-, and Q-band

Lucas R. Hunt[1,2], Aletha de Witt[3], David Gordon[2], Christopher S. Jacobs.[4], Megan C. Johnson[2]

Abstract We have undertaken an exploratory Q-band (43 GHz) imaging-astrometry project targeting the K-band ICRF sources in three sessions each of 24 hours using the Very Long Baseline Array. The project's goal is to compare images and astrometry from X, K, and Q-bands in order to study the optimal frequency band for CRF observations. The sources were observed as closely as possible in time, typically within a week, in order to minimize temporal variations in source structure. We will show how source structure compares between all three bands and show the interplay between source structure, resolution, and astrometry. We hope to use the results from our campaign to determine if pursuit of a Q-band CRF is worthwhile.

1 Introduction

The third realization of the International Celestial Reference Frame (ICRF3) was the first to be defined at three bands: S/X (2.3/8.4 GHz), K (24 GHz), and X/Ka (8.4/32 GHz) bands [2]. The two higher frequency reference frames allow for higher resolution, and with enough observations, higher positional precision. Sources in the higher frequency reference frames can also be used as calibrators when observing other objects (e.g. water masers at K-band) [6] and for Ka-band spacecraft navigation [8]. The first set of observations for the K-band realization of ICRF3 used the Very Long Baseline Array (VLBA) in 2002 and also included observations used to generate a reference frame solution at Q-band (43 GHz) [7].

The Q-band observations were initially paired with K-band observations, where a source was observed at K-band then Q-band with a short pause in the middle. It was an unsuccessful attempt to use data from the two frequency bands to remove ionospheric effects from the group delay measurement [7]. Positions were determined for 131 of the 172 sources observed at Q-band, for a success rate of $\sim$76%. As mentioned above, the K-band observations eventually became part of ICRF3, but the Q-band observations were the only observations of their kind.

The VLBA has improved data recording rates from 128 Mbps to 4,096 Mbps since the initial observations were taken in 2002 and 2003, and we were inspired to revisit the possibility of generating a reference frame solution at Q-band. A Q-band reference frame is tempting because the higher resolution at higher frequencies would allow for a more precise reference frame with enough observations. We need to determine if enough sources are visible at Q-band to generate a reference frame and if the higher resolution breaks up sources into multiple components where it would be difficult to determine a single position [4]. To assess the viability of a Q-band reference frame, we observed K-band ICRF3 sources at S-, X-, K-, and Q-band (S-band was omitted from this analysis in the interest of time). Our goal was to determine how many sources we might be able to detect and how source structure varies between the different frequency bands. In §2 of this paper, we describe the observations, calibration, and imaging of the data. In §3 we outline our findings from the imaging. Finally in §4 we provide a summary.

1. Computational Physics Incorporated
2. United States Naval Observatory
3. South African Radio Astronomy Observatory
4. NASA Jet Propulsion Laboratory, California Institute of Technology

2 Data

The observations were made using the VLBA [9] with a different set up for each observed frequency. See Table 1 for in depth details on the observing setup. Each experiment ran for 24 hours, with the X-band occurring on 16 April, 24 May, and 13 June using the VLBA's dichroic system, K-band observations occurring on 18 April, 23 May, and 12 June, and Q-band observations occurring on 19 April, 25 May, and 13 June.

The schedules were written using the scheduling program SCHED[1] using the hour angle selection mode in order to do both astrometry and imaging. To optimize imaging, most sources were visited in three scans per observation with a scan length of 1.5 minutes, while new sources had a scan length of 2 minutes. Figure 1 shows the number of sources targeted and imaged in each observation.

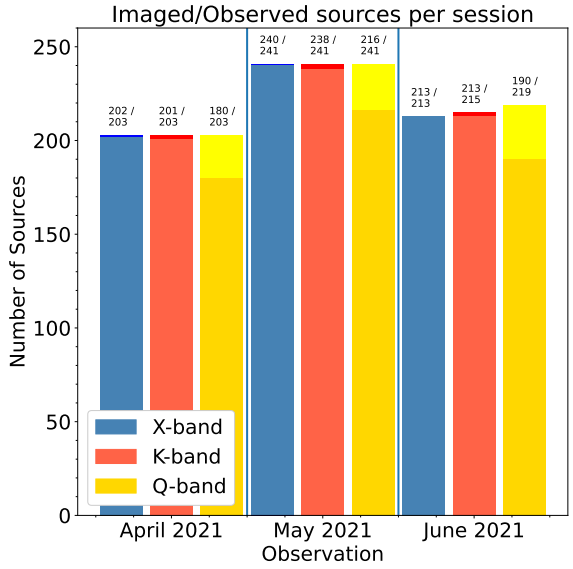

Fig. 1 The number of sources observed in each session. The X-band data is always in blue, the K-band data in red, and the Q-band data in yellow. The numbers above each bar indicate the number of sources imaged on the top and the number of sources observed on the bottom. The different shades of color for each bar also represent the number of sources observed and the number of sources imaged in each session.

The data were calibrated using NRAO's Astronomical Image Processing System (AIPS; [5]) following standard calibration procedures. More details will be available in [3]. The calibrated data were then split into individual source files and imaged using Difmap [10]. The imaging process started with a point source model, and iterated through a CLEAN and self-calibration cycle until the residual image was noise-like.

3 Analysis

In the end we targeted 453, 454, and 458 unique sources at X-, K-, and Q-band respectively. We successfully imaged 406, 449, and 452 sources, successfully detecting 99.7%, 98.9%, and 88.6% of sources at X-, K-, and Q-band respectively. This is an improvement over the $\sim$76% of sources detected in the original Q-band reference frame experiments [7]. Distribution of total flux density for each source is shown in Figure 2. The median clean fluxes are 338, 293, and 215 mJy and the mean clean fluxes are 657, 648, and 439 mJy at X, K, and Q-bands, respectively. Sources are fainter at higher frequencies but are still bright enough at Q-band that we are able to detect a significant fraction of sources. This indicates that there are likely enough sources to generate a robust reference frame at higher frequencies.

For the rest of the analysis we used a subset of 249 sources with an image quality parameter greater than 0.6 in the three frequency bands in order to minimize the corruption of the comparison from poor data. The image quality was determined using the average of the visibility fraction, resolution fraction, beam fraction, and error fraction. For more information on how these are calculated see deWitt et al. (submitted). We used these images to compare source compactness at different frequencies.

We first looked at compactness by dividing the peak flux by the total flux of the image where the peak flux is the flux density of the brightest pixel in Jy bm^{-1} and the total flux is the sum of the flux of all clean components output from the imaging procedure. If the object was completely point-like, the flux in the image would be in the brightest pixel. The ratio of the peak to total flux tells us how much of the total flux is in the brightest pixel and therefore how point-like the source is. Figure 3 shows the distribution of the peak-to-total flux. The mean values are 0.804, 0.769, and 0.761 at

[1] http://www.aoc.nrao.edu/software/sched/

Table 1 Observation setup.

All Sessions			
Parameter	Q-Band	K-Band	X-Band
Backend System	DDC[1]	DDC[1]	PFB[2]
Total channel windows	4	4	12
Single channel window bandwidth (MHz)	128	128	32
No. of spectral channels per window	256	256	64
Total bandwidth (MHz)	512	512	384
Frequency resolution (MHz)	0.5	0.5	0.5
Polarization	Dual	Dual	RR
Data rate (Gbps)	4	4	2
Sampling resolution (bits)	2	2	2
Channel Frequencies (MHz)	42976.5, 43104.5, 43232.5, 43360.5	23375.75, 23503.75, 23631.75, 23759.75	8443.875, 8475.875, 8507.875, 8539.875, 8603.875, 8635.875, 8699.875, 8731.875, 8795.875, 8827.875, 8859.875, 8891.875

[1]Digital Downconverter
[2]Polyphase Filterbank

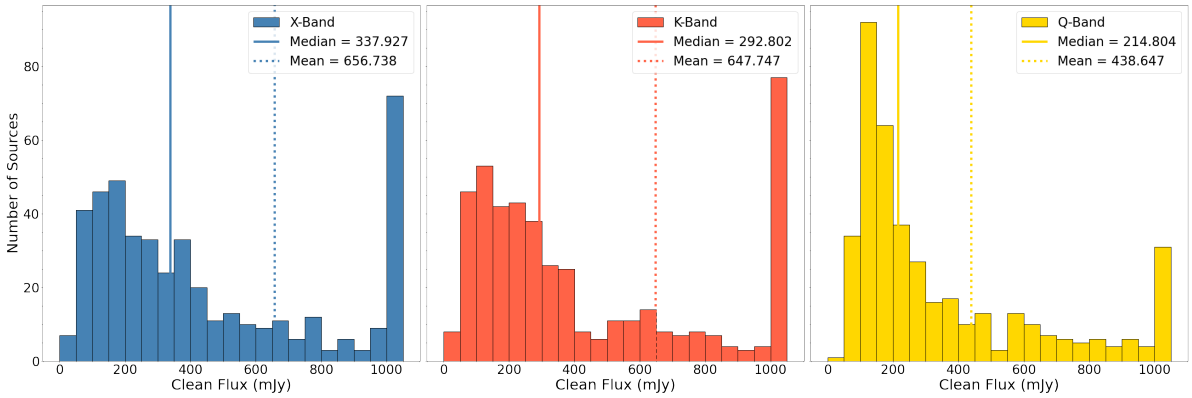

Fig. 2 Distribution of clean flux in sources detected at each frequency. X-band sources are in blue, K-band sources are in red, and Q-band sources are in yellow. All sources brighter than 1000 mJy are included in the bin furthest to the right of each plot, and the median and the mean of the distributions are shown by the solid and dashed lines respectively.

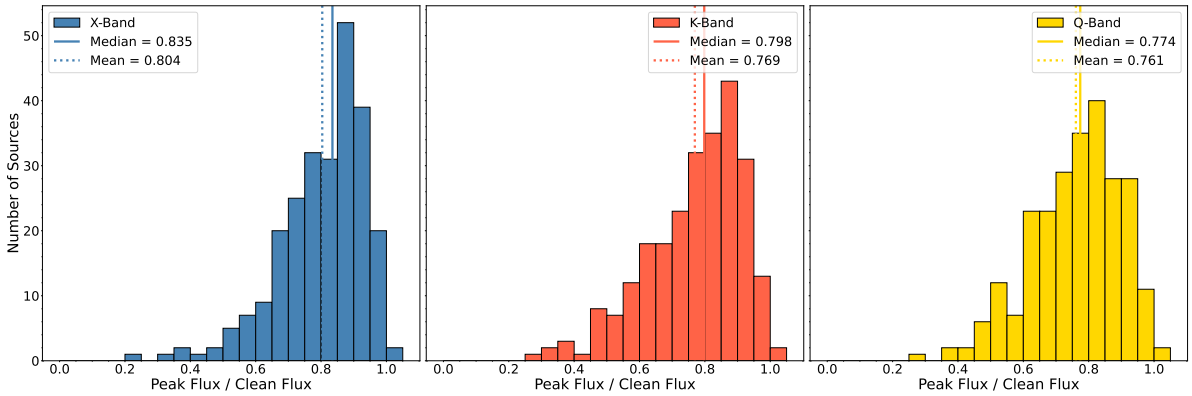

Fig. 3 Distribution of the ratio of peak flux to clean flux. X-band sources are in blue, K-band sources are in red, and Q-band sources are in yellow. The median and the mean of the distributions are shown by the solid and dashed lines respectively.

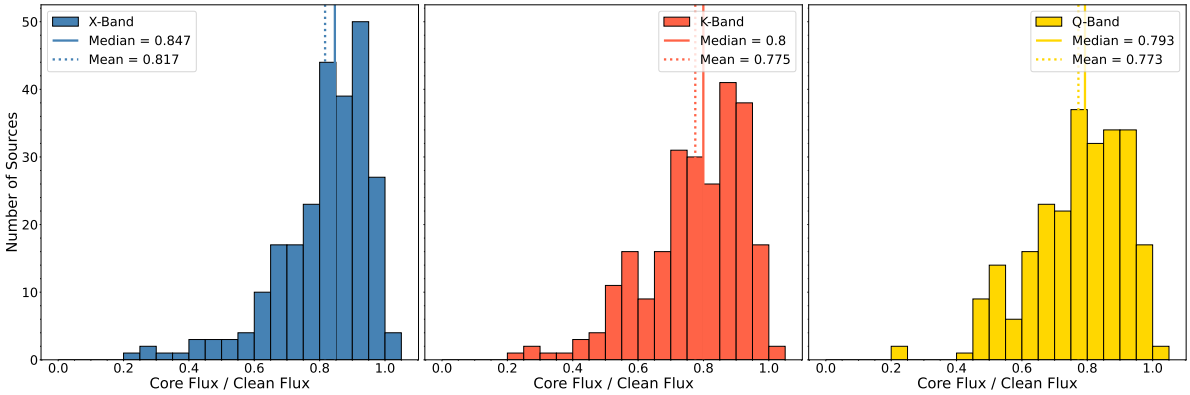

Fig. 4 Distribution of the ratio of core flux to clean flux. X-band sources are in blue, K-band sources are in red, and Q-band sources are in yellow. The median and the mean of the distributions are shown by the solid and dashed lines respectively.

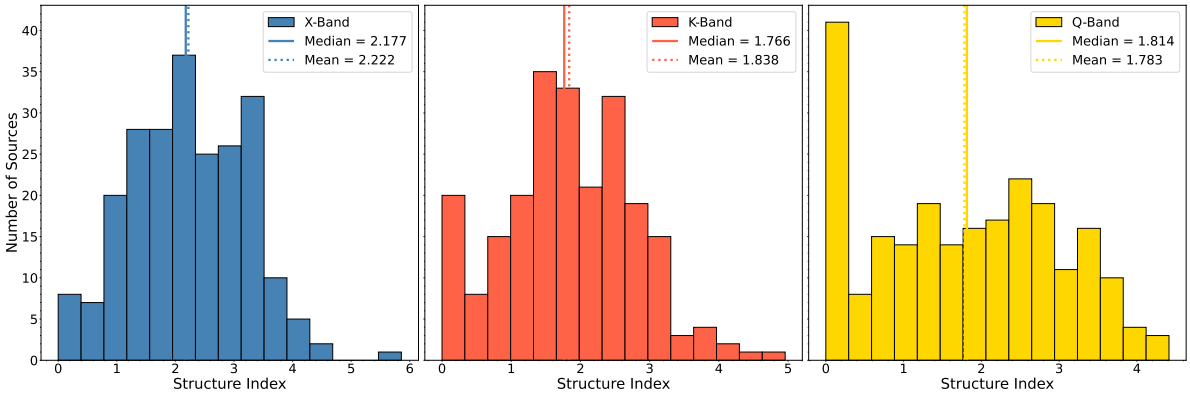

Fig. 5 Distribution of the source structure index. X-band sources are in blue, K-band sources are in red, and Q-band sources are in yellow. The median and the mean of the distributions are shown by the solid and dashed lines respectively. The source structure index is calculated using the logarithmic function, which means that values for the source structure index can be negative. In the case that a source structure index value is negative, we set that value to zero.

X-, K-, and Q-band, respectively, where values closer to 1 indicate a source is more compact.

Next we measured the core flux divided by the clean flux for each image. The core flux is defined as the sum of the clean components within a single beam on a global baseline. Again, the more flux concentrated at the center, the more compact the source is. The frequency of observation determines the beam size, so the core size is different for each frequency band. The beam is 0.71, 0.27, and 0.14 mas for X-, K-, and Q-band respectively. The distribution of core flux to clean flux ratio is shown in Figure 4. The mean value of this ratio is 0.817, 0.775, 0.773 for X-, K-, and Q-band respectively where values closer to 1 indicate a source is more compact.

We finally use the source structure index [1] to determine compactness. The source structure index is the log of the median value of the structure delay corrections derived from Very Long Baseline Interferometry (VLBI) images plus a constant. A higher structure delay indicates there is structure outside of the brightest component, meaning that the source is less compact. The mean values are 2.22, 1.84, and 1.78 for X-, K-, and Q-band, respectively, where lower values indicate that a source is more compact. We note here that we revisited our calculation of the source structure index and were able to fix an error. The distribution in Figure 5 shows the data from the updated calculations.

The peak flux over total flux ratio and the core flux to clean flux ratio show similar distributions across all three bands. The distributions of X-band and K-band

sources typically have a slightly higher mean, indicating the sources are more compact than at Q-band.

The distribution of values for the source structure index seems to show that many Q-band sources actually have a lower source structure index and are as compact at Q-band as they are at K-band. The average source structure index at X-band is slightly higher.

4 Conclusions

In this report we have discussed our exploration of K-band ICRF3 sources at X-, K-, and Q-band. We have shown that we can detect 99% of K-band ICRF3 sources at X and K-band and 87% of K-band ICRF3 sources at Q-band. We see that sources are generally fainter at Q-band, and that is likely the reason we don't detect as many. Finally, our results show nearly equal compactness at all three bands. The compactness is scaled by the beam and therefore by the inverse of the frequency. Thus, our results suggest the potential for improving the VLBI-defined ICRF by moving to higher frequencies and suggest that the improvements scale with frequency, i.e., Q-band is five times better in astrometric precision than X-band.

Acknowledgements

The authors acknowledge use of the Very Long Baseline Array under the US Naval Observatory's time allocation. This work supports USNO's ongoing research into the celestial reference frame and geodesy. The VLBA is operated by the National Radio Astronomy Observatory, which is a facility of the National Science Foundation operated under cooperative agreement by Associated Universities, Inc. The research was carried out in part at the Jet Propulsion Laboratory, California Institute of Technology, under a contract with the National Aeronautics and Space Administration (80NM0018D0004). Copyright 2022 All Rights Reserved. The financial assistance of the South African Radio Astronomy Observatory (SARAO) towards this research is hereby acknowledged.

References

1. Charlot, P. 1990. Radio-Source Structure in Astrometric and Geodetic Very Long Baseline Interferometry. The Astronomical Journal 99, 1309. doi:10.1086/115419.
2. Charlot, P. and 19 colleagues 2020. The third realization of the International Celestial Reference Frame by very long baseline interferometry. Astronomy and Astrophysics 644. doi:10.1051/0004-6361/202038368.
3. Aletha de Witt, Christopher S. Jacobs, David Gordon, Michael Bietenholz, Marisa Nickola, and Alessandra Bertarini 2022 The Astronomical Journal. Submitted.
4. Fomalont, E., Johnston, K., Fey, A., Boboltz, D., Oyama, T., Honma, M. 2011. The Position/Structure Stability of Four ICRF2 Sources. The Astronomical Journal 141. doi:10.1088/0004-6256/141/3/91.
5. Greisen, E. W. 2003. AIPS, the VLA, and the VLBA. Information Handling in Astronomy - Historical Vistas 285, 109. doi:10.1007/0-306-48080-8_7.
6. Immer, K., Reid, M. J., Menten, K. M., Brunthaler, A., Dame, T. M. 2013. Trigonometric parallaxes of massive star forming regions: G012.88+0.48 and W33. Astronomy and Astrophysics 553. doi:10.1051/0004-6361/201220793.
7. Lanyi, G. E. and 12 colleagues 2010. The Celestial Reference Frame at 24 and 43 GHz. I. Astrometry. The Astronomical Journal 139, 1695–1712. doi:10.1088/0004-6256/139/5/1695.
8. Morabito, D. D. 2017. Deep-Space Ka-Band Flight Experience. Interplanetary Network Progress Report 42-211, 1–16.
9. Napier, P. J. and six colleagues 1994. The Very Long Baseline Array. IEEE Proceedings 82, 658–672. doi:10.1109/5.284733.
10. Shepherd, M. C. 1997. Difmap: an Interactive Program for Synthesis Imaging. Astronomical Data Analysis Software and Systems VI 125, 77.